



Isostasy, flexure, and dynamic topography



Zohar Gvirtzman^{a,b,*}, Claudio Faccenna^c, Thorsten W. Becker^d

^a Geological Survey of Israel, Jerusalem, Israel

^b Institute of Earth Sciences, Hebrew University, Jerusalem, Israel

^c Dipartimento Scienze, Università Roma TRE, Rome, Italy

^d Department of Earth Sciences, University of Southern California, Los Angeles, California, USA

ARTICLE INFO

Article history:

Received 12 January 2016

Received in revised form 26 May 2016

Accepted 27 May 2016

Available online 31 May 2016

Keywords:

Topography

Isostasy

Dynamic topography

Crust

Lithosphere

Middle East

ABSTRACT

A fundamental scientific question is, what controls the Earth's topography? Although the theoretical principles of isostasy, flexure, and dynamic topography are widely discussed, the parameters needed to apply these principles are frequently not available. Isostatic factors controlling lithospheric buoyancy are frequently uncertain and non-isostatic factors, such as lithospheric bending towards subduction zones and dynamic topography, are hard to distinguish. The question discussed here is whether a set of simple rules that relate topography to lithospheric structure in various tectonic environments can be deduced in a way that missing parameters can be approximated; or does each area behave differently, making generalizations problematic. We contribute to this issue analyzing the Asia–Africa–Arabia–Europe domain following a top-down strategy. We compile a new crustal thickness map and remove the contribution of the crust from the observed elevation. Then, the challenge is to interpret the residual topography in terms of mantle lithosphere buoyancy and dynamics. Based on systematic relationships between tectonic environments and factors controlling topography, we argue that crustal buoyancy and mantle lithospheric density can be approximated from available geological data and that regions near mantle upwelling or downwelling are easily identified by their extreme residual topography. Yet, even for other areas, calculating lithospheric thickness from residual topography is problematic, because distinguishing variations in mantle lithosphere thickness from sub-lithospheric dynamics is difficult. Fortunately, the area studied here provides an opportunity to examine this issue. Based on the conjunction between the Afar Plume and the mid-ocean ridge in the nearby Gulf of Aden and southern Red Sea, we constrain the maximal amplitude of dynamic topography to ~1 km. This estimate is based on a narrow definition of dynamic topography that only includes sub-lithospheric processes and using mid-ocean ridges as reference, where mantle lithosphere buoyancy is zero.

© 2016 Elsevier B.V. All rights reserved.

1. Introduction

A fundamental question in earth sciences is, what controls the topography of the Earth's surface? Despite the basic observation that changes in topography are generally accompanied by changes in crustal thickness (e.g., Heiskanen and Vening Meinesz, 1958) that supports the paradigm of isostasy (Airy, 1855; Dutton, 1882), comparing presently available crustal thickness data with topography indicates a poor correlation (cf. Zoback and Mooney, 2003; Fig. 1). The reason for that is that the principle of isostasy does not apply to a crust floating on lava, as envisioned by Airy (1855), but to a relatively hard lithosphere floating on viscid asthenosphere. In other words, the modern paradigm of isostasy implies that topography depends on lithospheric buoyancy, which depends both on the crust and on the mantle lithosphere (ML) (e.g., Thompson and Talwani, 1964; Haxby and Turcotte, 1978; Davies, 1979; Lachenbruch and Morgan, 1990).

Other exceptions from a simple Airy-type model are narrow topographic loads that are not accompanied by local crustal thickening. These loads are supported by the strength of the lithosphere, which does not bend easily (e.g., Watts, 2001, and references therein). In other words, narrow topographic loads do not cause local sinking of the crust into the mantle or local sinking of the lithosphere into the asthenosphere, but produce a gentle flexure spreading over wide areas. Accordingly, isostatic equilibrium is usually maintained regionally over distances of 100–200 km, which is commonly the flexural wavelength of the lithosphere (e.g., Watts, 2001). In cases of cold and strong plates, flexure is considerably wider, particularly, in foreland and forearc basins (e.g., the north Indian Plate bending towards the Himalayas) that are strongly pulled down by far-off subducting slabs (Royden, 1993; Gvirtzman and Nur, 1999, 2001).

Another important process influencing Earth's topography on a scale of hundreds of kilometers is dynamic topography, which is a term that is used differently in the literature, but shall here indicate surface undulations caused by present-day mantle flow (e.g., Hager et al., 1985; Cazenave et al., 1989; Colin and Fleitout, 1990; Gurnis, 1993; Forte

* Corresponding author at: Geological Survey of Israel, Jerusalem, Israel
E-mail address: Zohar@gsi.gov.il (Z. Gvirtzman).

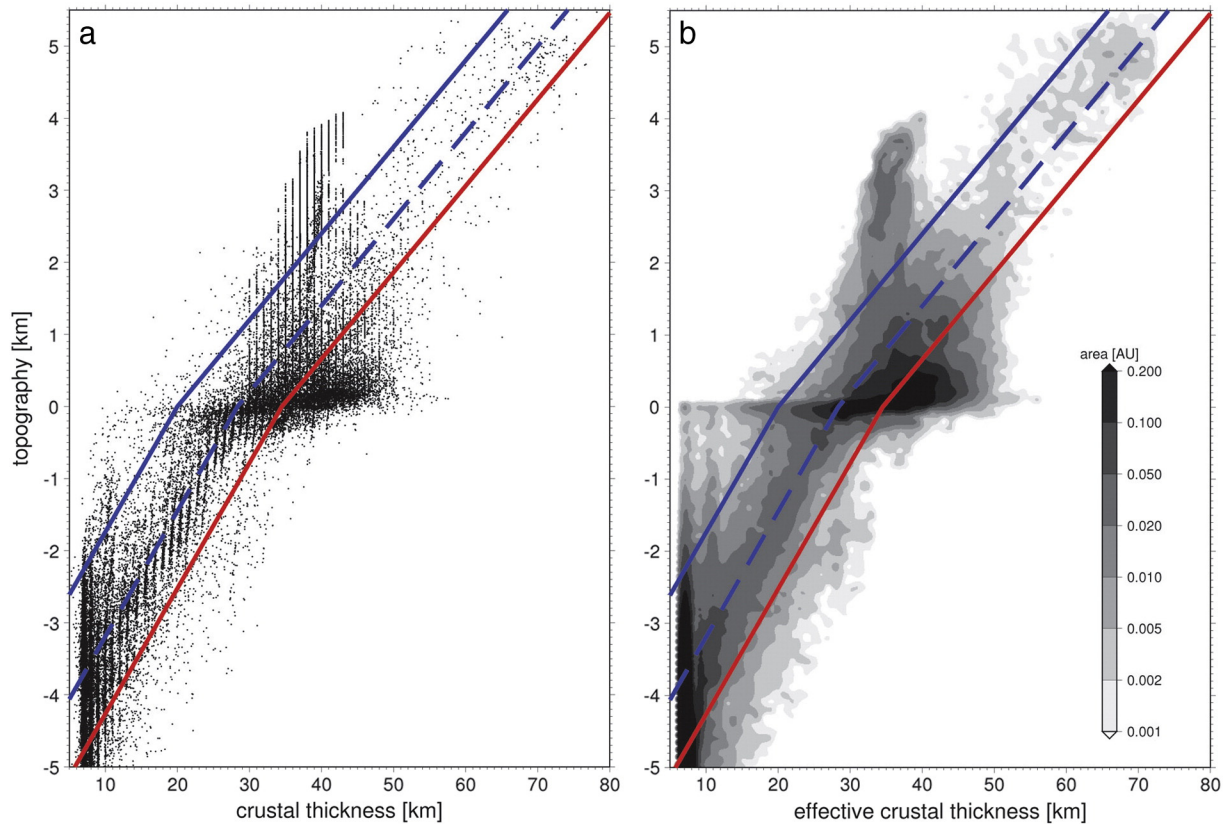


Fig. 1. Topography versus crustal thickness. (a) Original thickness grid points from the global CRUST1.0 model vs. median ETOPO1 topography, registered on the same 1×1 degree grid. Note that many negative topography (oceanic) values are based on an isostatic model within CRUST1.0, rather than data. (b) Smoothed representation of CRUST1.0 when thickness is sampled by even area distributed points and crustal thickness is normalized by model density variations (effective thickness = $L_c \rho_c / \bar{\rho}_c$). Gray shading indicates density of points within the axes domain represented by a log color scale proportional to relative area (arbitrary units). Blue line is topography predicted from crustal buoyancy. Dashed blue line is the same with a -1.1 km shift corresponding to negative buoyancy of a 100-km-thick ML assuming a density factor of -0.01 . Red line is the same as the blue line with a -1.74 km shift taken from Zoback and Mooney (2003). Note that many continental areas have a typical crustal thickness of ~ 35 km, but a large range of elevations. This indicates large deviations from isostasy, whereas the trend of the more extreme values validates the general concept.

et al., 1993; Le Stunff and Ricard, 1995; Thoraval et al., 1995; Christensen, 1998; Lithgow-Bertelloni and Silver, 1998; Gurnis et al., 1998; Daradich et al., 2003; Forte, 2007; Faccenna and Becker, 2010; Moucha and Forte, 2011; Becker et al., 2014). In this term, *dynamic* refers to moving mass anomalies unlike *isostasy* that refers to quasi-static mass anomalies. Note, however, that whether or not lithospheric-scale processes, such as small-scale convection in the thermal boundary layer and cooling of plates as they move away from spreading centers, are included in *dynamic topography*, is controversial (e.g., Gurnis, 1993; Forte et al., 1993; Flament et al., 2013; Becker et al., 2014; Faccenna et al., 2014a). Here, we use a narrow definition of dynamic topography that only includes sub-lithospheric processes (e.g., Le Stunff and Ricard, 1995; Panasyuk and Hager, 2000; Flament et al., 2013). Accordingly, lateral variations in lithospheric thickness are considered here isostatic though its deformation is dynamic (e.g., Faccenna et al., 2014b).

Topography of a certain region hence depends on quite a few factors controlling the buoyancy of the lithosphere (density and thickness of the crust and ML); the strength of the lithosphere (temperature, composition, etc.); the existence of adjacent loads that may be a few hundred km away (subducting slabs); and on many other factors controlling mantle dynamics. Hence, the ability to generate a simple basic law for a fundamental feature of the Earth, namely, its topography, is problematic.

Theoretically, the physical principles controlling topography were quantified in many fundamental studies (e.g., above references) and, given enough information, topography can be predicted. In practice, however, in most regions of the world, all the parameters that are

needed for those calculations are not available. So, the practical question becomes whether a set of useful and simple rules that relate topography to lithospheric structure in various tectonic environments can be deduced in a way that missing parameters can be guessed reasonably well; or does each area behave differently.

In a previous study (Zoback and Mooney, 2003) that used 1700 crustal structure profiles from the global database compiled by the U.S. Geological Survey (Mooney et al., 2002), crustal contribution to topography was shown to be always much higher than the observed topography. Zoback and Mooney (2003) explained that the negative buoyancy of the ML lowers the observed topography by 1.73 km on average (Fig. 1). Moreover, they computed the thickness of the ML for each point in their dataset and showed that lithospheric thickness deduced from isostasy generally agrees with seismic data.

However, the individual analysis of each data point still does not reduce the scatter covering the crustal thickness–topography diagram (Fig. 1). Can we explain the distribution of points within this cloud? Can we distinguish clusters related to distinct tectonic environments as shown by Hyndman and Currie (2011) for North Western America (hot Cordillera vs. cold craton)? Or is it too complex for any useful global rules?

This study tries to answer these questions emphasizing the phenomenology. For this purpose, we chose the Mediterranean–Red Sea domain (Fig. 2), which includes a variety of tectonic environments: inter- and intra-plate regions, active and passive continental margins, and cool versus hot mantle regions. We examine the relationships between tectonic setting and crustal density, strive to remove the contribution of the crust from the observed elevation, and interpret the residual

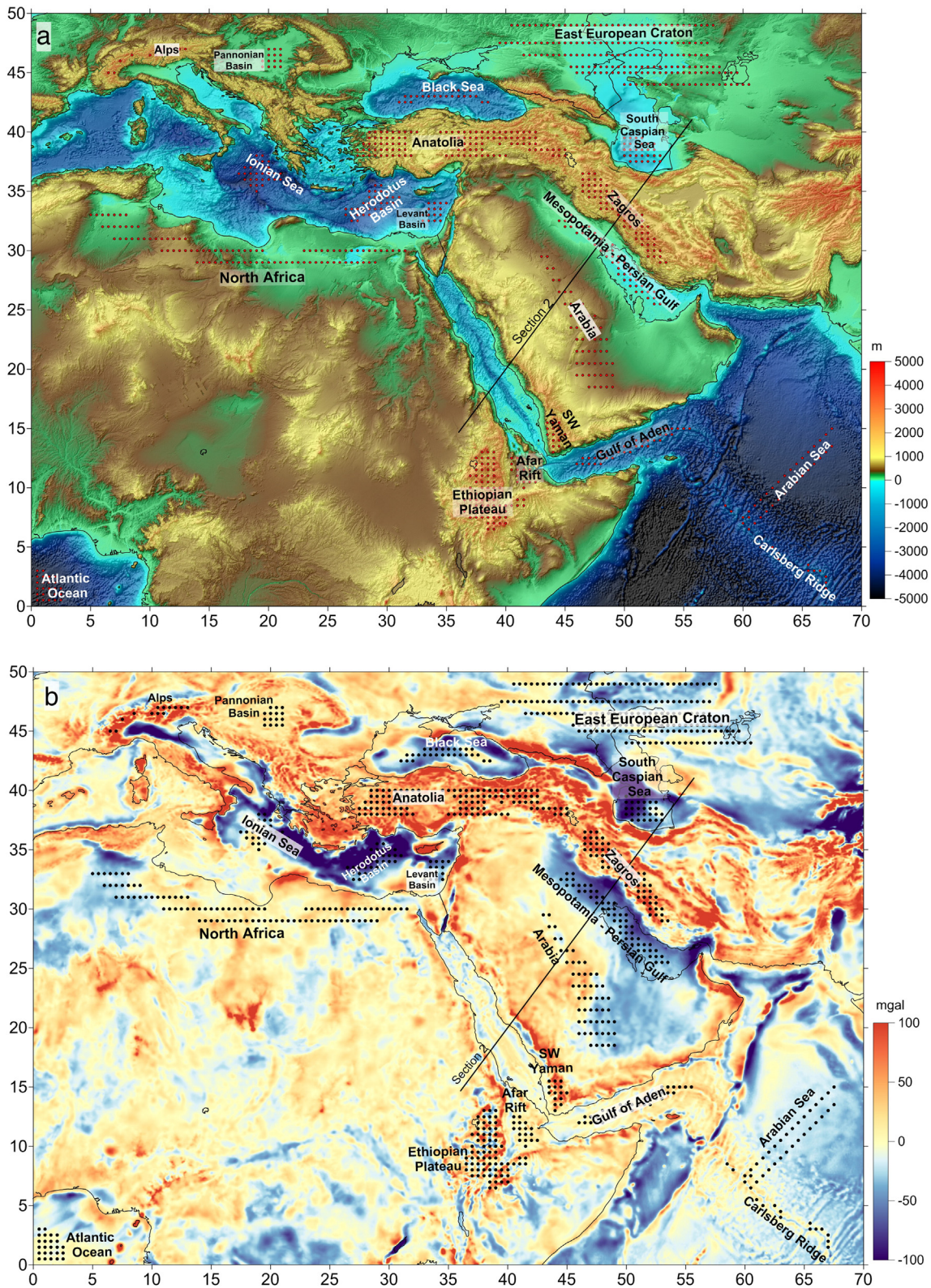


Fig. 2. Location map with (a) topography from ETOPO1 (Amante and Eakins, 2009) and (b) Free Air Gravity from Sandwell and Smith (2009). Black dots are locations within 20 selected tectonic environments that were specifically analyzed. Straight line marks the track of Section 2 (Fig. 9).

topography in terms of ML buoyancy, plate bending, and dynamics. Based on the conjunction between the Afar Plume and the mid-ocean ridge in the nearby Gulf of Aden and southern Red Sea, we constrain the amplitude of dynamic topography. Based on understanding the lithospheric structure in the Mesopotamian, Ionian, and Herodotus basins,

we constrain the amplitude of the downward pull force exerted by subduction (flexure and dynamic topography).

In addition to the general contribution of this study to the issue of isostasy and topography, the distinction between static and dynamic processes in the Red Sea–Middle East–Mediterranean domain is of

special interest. In this part of the world, dynamics is related to mantle flow from the Afar plume in East Africa, through the Middle East, all the way to Anatolia and the Aegean Sea (Daradich et al., 2003; Forte et al., 2010; Chang and Van der Lee, 2011; Becker and Faccenna, 2011; Faccenna et al. 2013, 2014a; Sembroni et al., 2016; Bar et al., 2016). Our analysis constrains the vertical effect of this dynamic flow.

2. Methodology

2.1. Formulation

The mean elevation ε , of a region depends on the local lithospheric buoyancy H , dynamic topography DT (e.g., upwelling mantle plume), and flexure FL . In this formulation, FL refers to short wavelength elastic flexure as well as to long wavelength inelastic bending of foreland and forearc basins caused by far-off subducting slabs.

$$\varepsilon = a(H + DT + FL), \quad (1)$$

$$a = \frac{\rho_a}{\rho_a - \rho_w} \quad \varepsilon \geq 0$$

$$a = \frac{\rho_a}{\rho_a - \rho_w} \quad \varepsilon < 0$$

where a expresses the deepening of ocean floor due to the water load; and ρ_a and ρ_w are the densities of the asthenosphere and water, respectively.

Considering that lithospheric buoyancy H , is a sum of contributions from the buoyancies of the crust (H_c) and the mantle lithosphere (H_{ml}), Eq. (1) can be expanded as

$$\varepsilon = a(H_c + H_{ml} - H_0 + DT + FL), \quad (2)$$

where H_0 is a constant that allows using sea level as a reference datum instead of a theoretical free asthenosphere surface. $H_0 = 2.4$ km makes Eq. (1) consistent with density and elevations of mid-ocean ridges (Lachenbruch and Morgan, 1990).

The quantities H_c and H_{ml} are defined as

$$H_c = \frac{1}{\rho_a}(\rho_a - \rho_c)L_c, \quad (3)$$

and

$$H_{ml} = \frac{1}{\rho_a}(\rho_a - \rho_{ml})L_{ml}, \quad (4)$$

where ρ_c , ρ_{ml} and L_c , L_{ml} are the mean densities and the thickness of the crust and the mantle lithosphere, respectively.

If the lithosphere consists only of crust (e.g., mid-ocean ridges), then $L_{ml} = 0$ and the elevation would be:

$$\varepsilon_c = H_c - H_0 \quad (5)$$

In cases of local isostatic equilibrium, here the dynamic and flexural components are negligible,

$$\varepsilon = a(\varepsilon_c + H_{ml}), \quad (6)$$

$$H_{ml} = \frac{\varepsilon}{a} - \varepsilon_c \quad (7)$$

and, thus, the thickness of the ML can be calculated:

$$L_{ml} = \frac{\rho_a}{(\rho_a - \rho_{ml})} \left(\frac{\varepsilon}{a} + H_0 - H_c \right), \quad (8)$$

Note that for this calculation, the ratio $\frac{\rho_a}{(\rho_a - \rho_{ml})}$ is the important factor rather than the absolute densities of the ML and asthenosphere. This

density ratio depends on the temperature difference between the hot asthenosphere and the cool ML (e.g., Parsons and Sclater, 1977):

$$\rho_{ml} = \rho_a [1 + \alpha(\theta_a - \theta_{ml})], \quad (9)$$

where θ_a and θ_{ml} are the temperatures of the asthenosphere and average ML, respectively, and α is the volume coefficient of thermal expansion. In this study, we use $\theta_a = 1350$ °C, $\alpha = 3.5 \cdot 10^{-5}$ °C⁻¹, and $\rho_a = 3190$ kg·m⁻³.

Assuming a linear geotherm for the ML, the average temperature of the ML is simply

$$\theta_{ml} = \frac{1}{2}(\theta_c + \theta_a), \quad (10)$$

where θ_c is the temperature at the Moho. Supplementary Fig. 1a illustrates that the average temperature, and accordingly density, of the ML is independent of its thickness, but only depends on the temperatures at its boundaries. In practice, thermal models of the crust or lithosphere commonly provide temperature maps at a constant depth (e.g., Artemieva, 2006) and not at the laterally varying Moho level. However, a first-order estimation of Moho temperature can be obtained from a simple linear approximation (Supplementary Fig. 1b). The error associated with this approximation is usually smaller than the uncertainty in the temperature data and its influence on density is quite small.

For the general case, in which DT and flexure cannot be ignored (in other words, isostatic equilibrium is not maintained locally and Eqs. (6)–(8) do not apply), subtraction of crustal buoyancy from the observed topography is termed residual topography, RT :

$$RT = \frac{\varepsilon}{a} + H_0 - H_c = H_{ml} + DT + FL \quad (11)$$

A main challenge of this study is to identify and constrain DT and FL where they are important and to allow a simple isostatic calculation of H_{ml} and L_{ml} in the rest of the world. For this we, first, show the results of an isostatic approach that interprets RT in terms of H_{ml} and L_{ml} limiting DT only to areas where isostasy alone cannot explain the observations (mantle plumes and subduction zones). Then, we discuss the error in L_{ml} associated with ignoring DT .

2.2. Research strategy

Currently, there is a significant difference between the quality and quantity of information about the crust and the information about the ML. This difference is partly related to the simple fact that the base of the crust is much shallower than the base of the lithosphere; but also to the somewhat vague nature of the lithosphere–asthenosphere boundary (LAB), which is gradual and definition dependent (discussion below).

Since the Moho is better defined than the LAB, we adopt a top-down strategy. We begin with the crust and remove its contribution to the observed topography and only then try to interpret the residual topography. Also, considering that with poor knowledge of Moho depth, our exercise is useless, our first effort is to improve the Moho map in the East Africa–Middle East region, where a lot of data not included in previously published datasets are available. We also paid special attention to the gridding method. Since, in many cases, data points are collected along roads crossing geological structures, automatic gridding wrongly connects data points across geological boundaries. Therefore, when necessary, we forced contours to follow topographic and geological strike lines. Lastly, we generated a grid of 0.5° spacing, averaging the topography of a few tens of kilometers for each node (later, when we interpret RT , we further smooth our results beyond a flexural wavelength of 100–200 km).

To better understand the relations between residual topography and tectonic environments, we focus on 20 regions: Gulf of Aden, Western

Yemen, Afar Rift, Ethiopian Plateau, Anatolia, Pannonian Basin, Carlsberg Ridge, Arabian Sea, Atlantic Ocean, Zagros, Alps, North Africa, Arabia, Levant Basin, Black Sea, Eastern European Platform, South Caspian Sea, Herodotus Basin, Ionian Basin, Mesopotamian Basin, and the Persian Gulf (Fig. 2b). We illustrate that the selected regions reveal a systematic order that is hard to distinguish otherwise.

A particular challenge is to interpret the residual topography. In areas of high RT, we need to distinguish between a static state of a thin lithosphere and a dynamic state of a lithosphere that is pushed up by an upwelling mantle flow. We use the southern Red Sea–Afar–Aden conjunction for that. In areas of low RT our challenge is to distinguish between the effect of a thick lithosphere and the down-bending of the lithosphere towards subduction. This discussion is

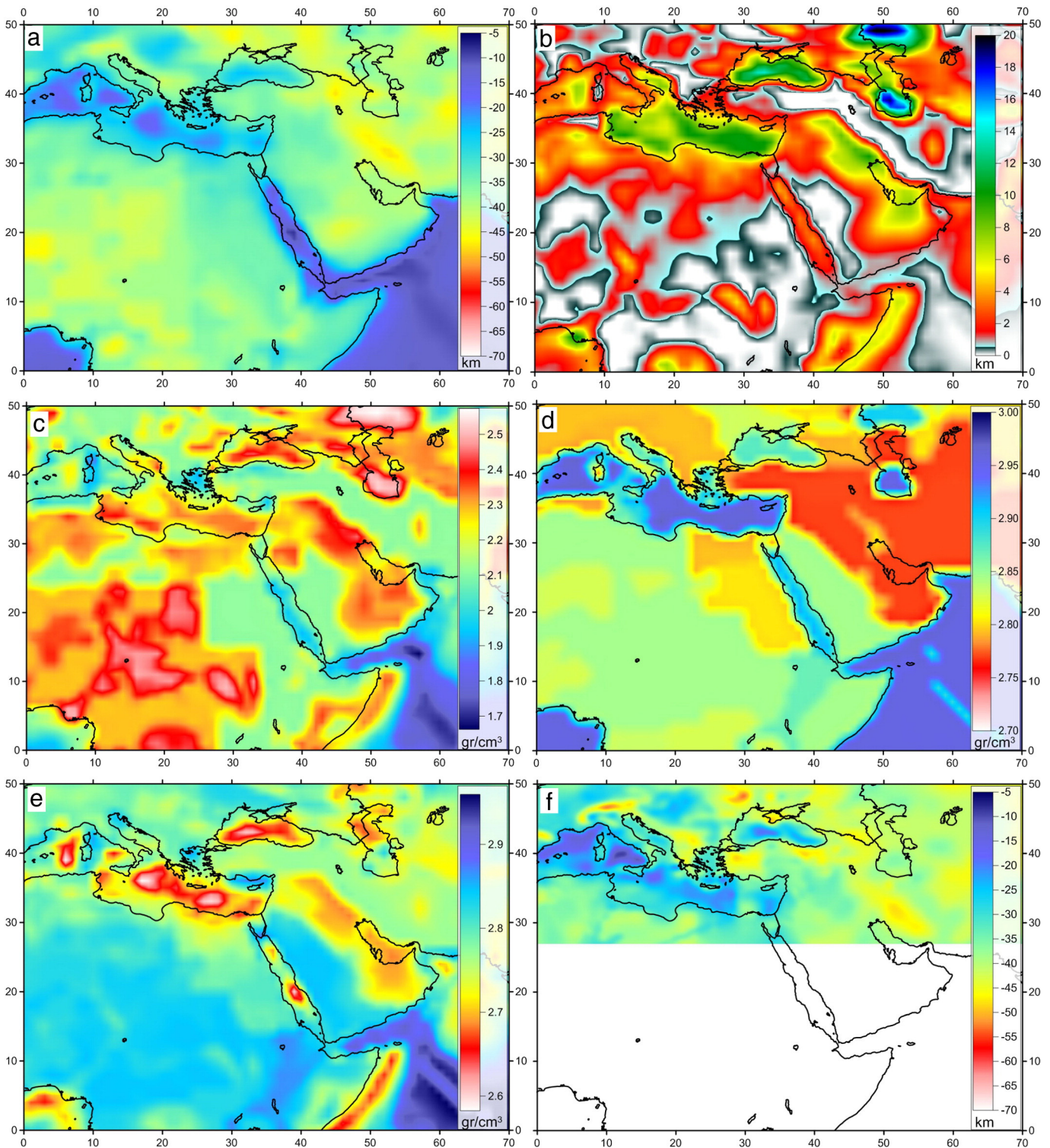


Fig. 3. Crustal datasets. (a) Moho depth. (b) Sediment thickness. (c) Average sediment density. (d) Average density of crystalline crust. (e) Average density of entire crust. (f) Moho depth for Europe. (a–e) taken from CRUST1.0 model (<http://igppweb.ucsd.edu/~gabi/rem.html>, Laske et al., 2013) and (f) from Grad and Tiira (2009).

illustrated on foreland basins. Lastly, we suggest several typical combinations of topography and lithospheric structures for various tectonic environments.

2.3. Data

Topography was taken from ETOPO1 which is a 1 arc-minute global model (Amante and Eakins, 2009; downloaded June 26, 2012). In order to avoid sharp topographic variations that are not compensated locally, we have generated a coarser topographic grid of 0.5° for buoyancy calculations.

As a starting point for the crust, we use CRUST1.0 (<http://igppweb.ucsd.edu/~gabi/rem.html>) (Laske et al., 2013), which is an update of CRUST2.0 (Bassin et al., 2000) and CRUST5.1 (Mooney et al. 1998), a global model of $1^\circ \times 1^\circ$ resolution with 8 layers, including Moho depth (Fig. 3a), sediment thickness (Fig. 3b), average sediment density (Fig. 3c), average crystalline crust density (Fig. 3d), and average crustal density (Fig. 3e). For Europe, we used the $0.1^\circ \times 0.1^\circ$ Moho map by Grad and Tiira (2009) (Fig. 3f).

Examining the crystalline crust density map of CRUST1.0 (Fig. 3e), we identify major variations that resemble those of the sediment thickness map (Fig. 3b). We suspect that these variations in the crystalline crust are not derived from measurements, but reflect residuals from sediment distribution. Thus, we prefer using a simplified model including only two types of crystalline crust (oceanic and continental) as shown below.

For our new compilation of crustal thickness in the East Africa–Middle East region, we attempted to collect all published data within the area marked in Fig. 4 by a polygon (details are in Supplementary

Table 1). We used seismic refraction surveys, receiver function Moho depth estimates, and in some places local Moho maps. We avoided using gravity-driven maps which are more interpretation-dependent and *a priori* assume isostatic equilibrium.

3. Results

3.1. New Moho map

Differences between our map (Fig. 4b) and previous compilations (Fig. 4a) which result from the new data we used are seen mainly in Anatolia, Iran, East Africa, and Yemen (references in Supplementary Table 1; new Moho grid in Supplementary 3). Other significant changes are related to the strategy of interpolation. For example, quite a few data points indicate a relatively thin crust (~ 30 km) in the south Caspian Sea a few hundred kilometers offshore. In addition, many other data points along the Alborz Mountain chain indicate a much thicker crust (~ 50 km). Automatic gridding yields a gradual transition along a few hundred kilometers, whereas we forced a sharp transition following the collisional plate boundary.

Another example is the Red Sea. Three clusters of data points are available in the north, central, and southern Red Sea. With the absence of additional data points along most of the Red Sea, automatic gridding will not generate a narrow elongated feature unless contours are forced to a Red Sea parallel trend. This problem increases when the resolution is too low to express changes detected along transect lines. For instance, the Moho map of CRUST1.0 (Fig. 3a) is not resolved enough to express the transition from mountains, to coast, to narrow shelf, and eventually to an oceanic spreading center. In our map, we forced an elongated

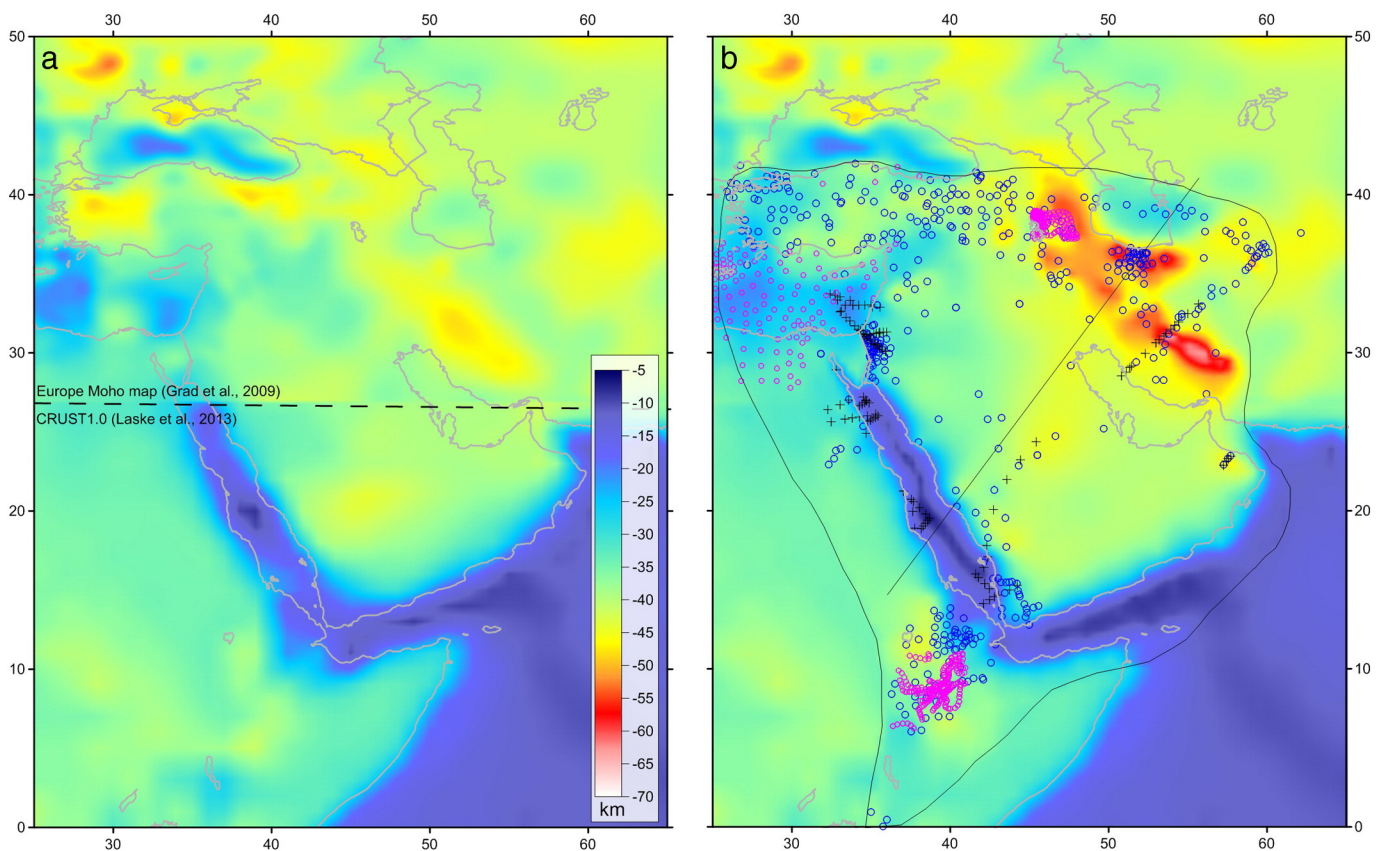


Fig. 4. Revised Moho map in the East Africa–Middle East region. (a) Moho map generated from CRUST1.0 (Laske et al., 2013) and Grad and Tiira (2009). (b) The new compilation of this study (marked by a polygon) embedded in previous models. Data points marked by black crosses are taken from seismic refraction lines, blue circles mark receiver function measurements, and magenta circles are points digitized from published Moho maps. Straight line marks the track of Section 2 (Fig. 9).

trend with an ~7-km-thick crust along the loci of spreading. Similarly, for the oceanic crust of the Gulf of Aden, we used a 7-km-thick crust where no other information exists as also seen in CRUST1.0.

Our map includes many other differences compared to previous compilations, for example, in the Levantine region (Syria, Lebanon, Israel, and Egypt) we distinguish the Lebanese and the Palmyrides

mountain chains, which are not recognized in CRUST1.0. Minor changes are also noticed in Israel and Jordan due to many receiver function estimates in that area.

We cannot accurately determine the errors in our new Moho map, because the needed information in the various sources we used is usually not available. Nonetheless, we estimate that the range of

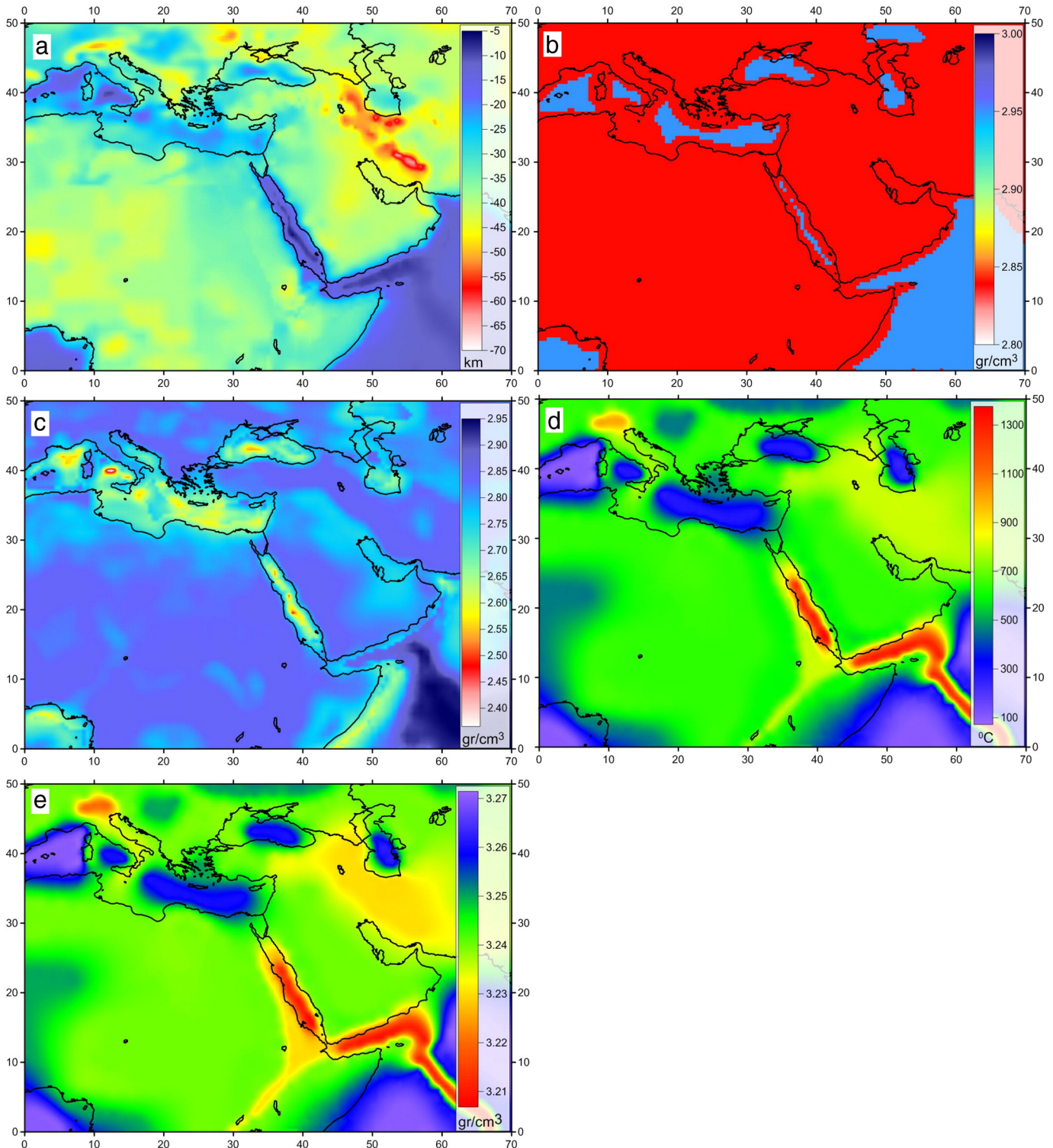


Fig. 5. Crustal data used in this study. (a) Moho depth (new grid in Supplementary 3), (b) simplified crystalline crust density: 2.84 cm^3 for continental crust and 2950 kg/m^3 for oceanic crust; (c) average crustal density, (d) Moho temperature, (e) average mantle lithosphere density.

uncertainty is 1–2 km for provinces with crustal thicknesses of 5–15 km; 2–3 km for 15–25 km; 3–4 km for 25–35 km; 4–5 km for 35–45 km; and 5–8 km for a 45- to 60-km-thick crust. A similar range

of uncertainty is described by Grad and Tiira (2009) for Europe (details in Fig. 4). In Central Africa (not crucial for our analysis), which was not included in our compilation and where crustal thickness is taken from

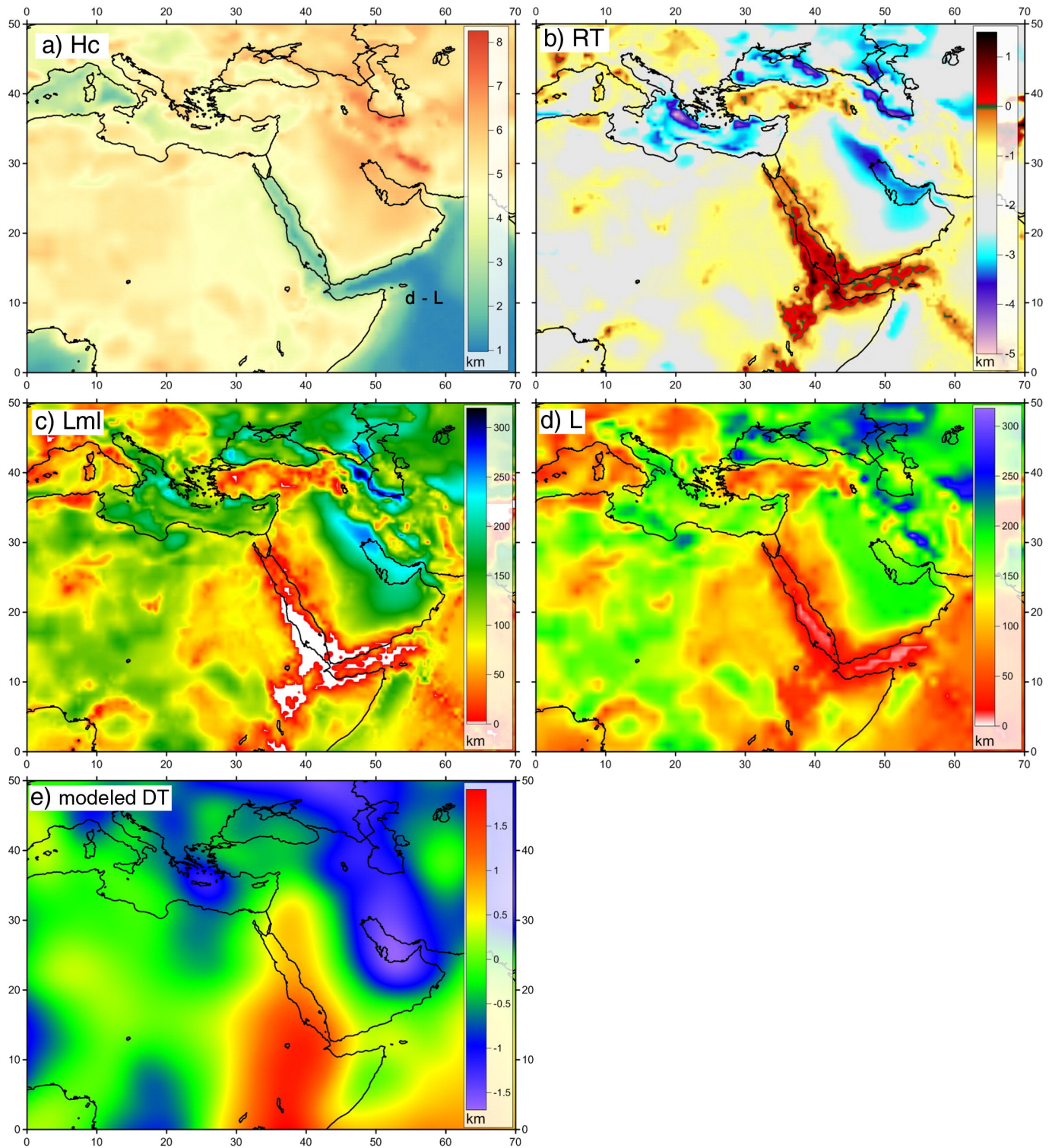


Fig. 6. (a) Crustal contribution to topography, H_c . (b) Residual topography RT. Dark blue and purple areas represent foreland and forearc basins (south Caspian, NE black sea, Mesopotamia, Herodotus, and Ionian basins), where RT is exceptionally low (< -3 km) coinciding with large negative free air anomalies (Fig. 2b). (c) ML thickness, L_{ml} , computed from residual topography. In foreland and forearc basins, the calculated thickness of the ML is unrealistically thick (>200 km). White area (positive RT) represents approximated zone with no ML. (d) Total lithospheric thickness inferred from residual topography. In forearc and foreland basins lithospheric thickness is taken from adjacent areas. In areas with no ML, lithospheric thickness equals crustal thickness. (e) Dynamic topography prediction from present-day mantle flow (from Faccenna et al., 2014a) using the SAVANI S-wave model (Auer et al., 2014). The computation infers topography from instantaneous flow and uses a simple, only radially variable viscosity structure which allows spectral solution via a code such as HC [Milner et al., 2009]. All density anomalies above 100 km depth are set to zero, and below Vs anomalies are scales as $d \ln \rho / d \ln V_s = 0.2$, for simplicity. Computation is the same as in Faccenna et al. (2014b) (see their Figure 14b for details). Noteworthy, this model shows similar trends as RT (b).

CRUST1.0, errors may be larger. Implications of crustal thickness uncertainties are discussed below.

3.2. Crustal density and temperature

Since we suspect that the density map for the crystalline crust in the CRUST1.0 model includes artifacts resulting from sediment

distribution, we prepared a simplified bi-modal distribution map: oceanic crystalline crust with an average density of 2950 kg/m^3 and continental crystalline crust with an average density of 2840 kg/m^3 (Fig. 5b). Combining this map and the sediment density map of CRUST1.0, we generated the average crustal density map of Fig. 5c, which slightly differs from the crustal density map of CRUST1.0 (Fig. 3e). The Moho temperature map of Fig. 5d was

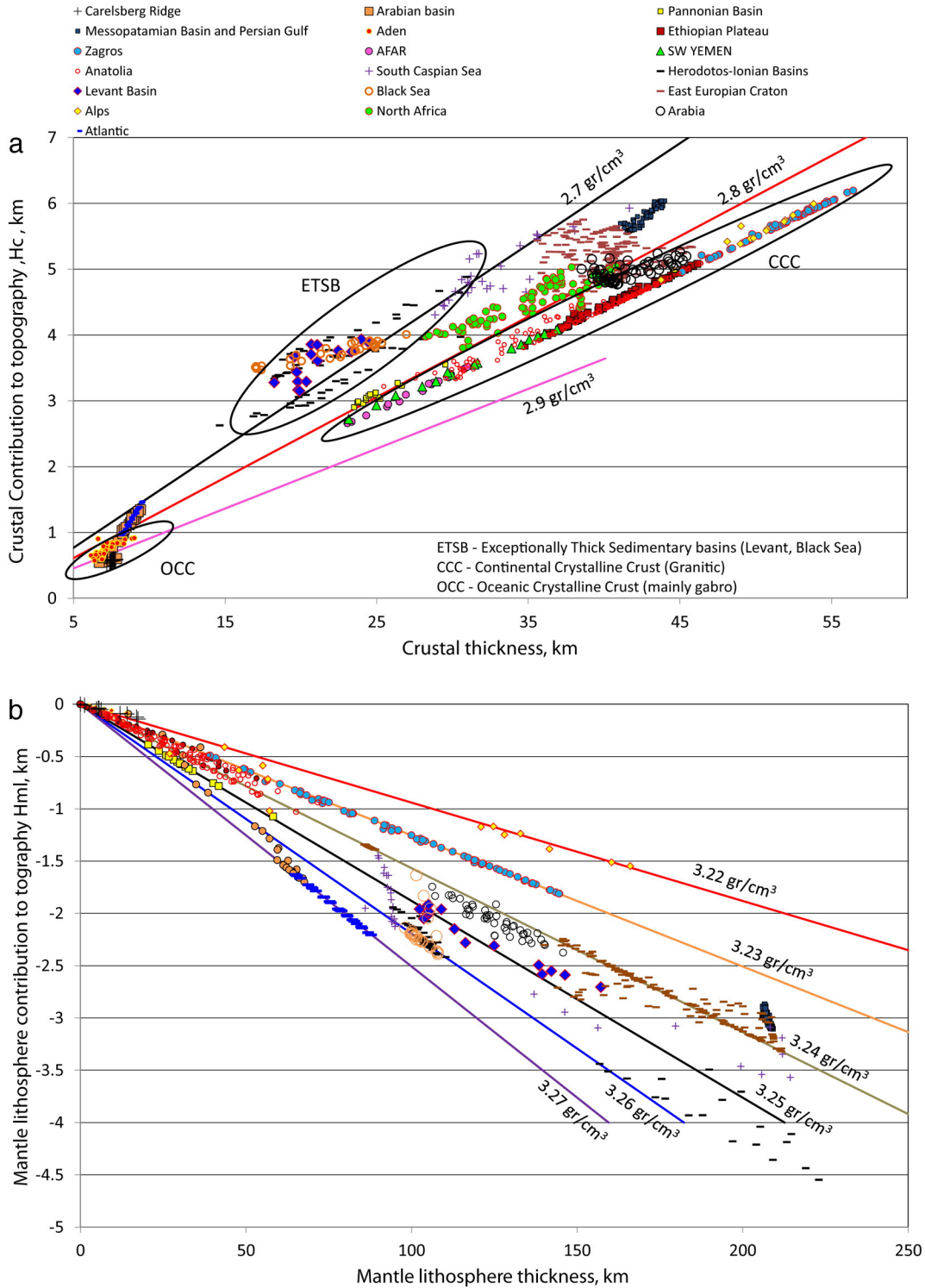


Fig. 7. Computed contributions of crust and ML to topography for selected tectonic environments. (a) Crustal contributions to topography as a function of crustal thickness and density, (b) ML contribution as a function of ML thickness and density. Note that ML thickness computed from residual topography reaches unrealistically thickness in forearc/foreland basins (see text).

derived from a constant 40 km depth temperature map of Artemieva (2006) corrected for the depth difference between 40 km and the local Moho. Lastly, the density of the ML was calculated from Moho temperature using Eqs. (9)–(10) (Fig. 5e).

3.3. Crustal contribution to topography

As expected, the main trend in the map of crustal contribution to topography H_c (Fig. 6a), resembles the main trends of the Moho map, but this does not allow identifying the influence of crustal density. To examine how big the density factor is, Fig. 7a plots H_c versus crustal thickness L_c , for 20 selected tectonic regions. Oceanic basins such as the Arabian Sea and Gulf of Aden with their thin sedimentary cover fall along the 2900 kg/m³ line, consistent with a nearly gabbroic crust. The Zagros, Alps, East Africa, Yemen, and Anatolia, fall between 2800 kg/m³ and 2900 kg/m³, consistent with a nearly granitic crust. Exceptionally thick sedimentary basins with a relatively thin crystalline crust, such as the Levant, Black Sea, Herodotus, and Ionian Basins, fall above the 2700 kg/m³ line, which is quite low for the Earth's crust.

This is a reminder that common density variations can easily influence Earth's topography by more than a kilometer and cannot be neglected. More encouraging, these variations can be estimated considering the tectonic environment, and specifically, the sedimentary cover and type of crystalline crust. Typical crustal density values are 2900 kg/m³ for oceanic basins with a thin sedimentary cover, 2850 kg/m³ for continental areas with a thick crust and thin sedimentary cover, 2750 kg/m³ for most sedimentary basins, 2650 kg/m³ for exceptionally thick sedimentary basins, where the less dense sediments significantly lower the crustal average, and a default common values of 2800 kg/m³ for all other regions. In other words, the uncertainty in crustal mean density should be in the order of the variance within each cluster of Fig. 7a, that is, ~50 kg/m³ for most provinces, ~100 kg/m³ in deep oceanic basins, where uncompacted sediments overly a dense gabbroic crust, and ~25 kg/m³ in regions of nearly pure continental crust.

Considering the range of uncertainty in crustal thickness and density, the uncertainty in H_c that is directly transferred to RT is in the order of ± 100 –500 m for regions with crustal thicknesses of 5–15 km (largest uncertainty in density, but small uncertainty in thickness); 400–700 m for 15–25 km; 700–1000 m for 25–35 km; 1000–1500 m for 35–45 km and also for 45- to 60-km-thick crust (largest uncertainty in thickness, but lesser uncertainty in density).

3.4. Residual topography

The residual topography map of Fig. 6b is dominated by hot colors expressing values between -1 km and 1 km and blue colors expressing values lower than -3 km. However, this situation is clearly abnormal. Empirically, the world average is -1.73 km (Zoback and Mooney, 2003) and, theoretically, the calculated buoyancy of 80- to 100-km-thick ML is between -1.0 km and -2.0 km (Fig. 3 of Lachenbruch and Morgan, 1990). In other words, only the gray regions in the RT map of Fig. 6b are “normal”, whereas most of the study area is higher or lower than expected from a stable isostatic lithosphere. The challenge now is to interpret the RT in this unique area and to distinguish between ML buoyancy and dynamic topography due to upwelling or to down-bending of the lithosphere towards subduction.

3.5. Residual topography and tectonic environments

To better understand the relations between residual topography and tectonic environments, we focus again on the 20 chosen tectonic areas (Fig. 8a). The first prominent observation is that positive RT is observed in Aden, Ethiopia, and SW Yemen, that is, around the upwelling Afar mantle plume. Positive RT cannot be related to the buoyancy of the

ML, which must be negative or zero where it does not exist (i.e., mid-ocean ridges like the Carlsberg Ridge).

The second prominent observation is that exceptionally low RT of -3 km to -5 km is observed in forearc (Ionian Basin and Herodotus Basin) or foreland basins (Mesopotamian Basin, Persian Gulf, and South Caspian Sea), where the lithosphere bends towards convergence plate boundaries. This bending perturbs the isostatic equilibrium as also indicated by exceptionally low free air gravity anomalies (Fig. 2b). Even in the Herodotus and Ionian basins, which probably have the oldest oceanic crust on Earth (Speranza et al., 2012), the exceptionally low RT is not explained by thermal cooling of the lithosphere because thermal cooling cannot contribute much more than 2 km of subsidence (not including water load) (Lachenbruch and Morgan, 1990) and hence the difference between 150 Ma and 250 Ma of cooling is no more than a few hundred meters.

Plotting residual topography against crustal thickness (Fig. 8b) shows that crustal thickness distinguishes between very thin (e.g., oceanic), thin (stretched continents), intermediate (common continents), and thickened (orogens) crust; and RT distinguishes between hot and cold regions. Such a diagram is useful for describing various geological environments and the amplitude of vertical motions transferring regions from one state to another (rifting, cooling, etc.).

Oceanic floor is generated at mid-ocean ridges (MOR) with no ML. Then, while moving away from the spreading center and cooling, their ML gradually thickens and its negative buoyancy increases. In terms of RT, these basins begin with RT = 0 (e.g., the Carlsberg Ridge excluding its northernmost segment), decreasing to RT of about -1 km to -1.5 km in Young Oceanic Basins (YOB) like the Arabian Sea, and then further decreasing to -2 km in Old Oceanic Basins (OOB) like the old Atlantic margins of West Africa. In view of this typical path, the Gulf of Aden is exceptional with its positive RT indicating DT.

Stretched continental basins (Afar and Pannonian, Levant, and Black Sea) begin their development as Young Rifted Basins (YRB) with a thin ML that subsequently cools, thickens, and increases its negative buoyancy. The young Pannonian Basin is characterized by RT of ~ -0.7 km. The older basins of the Black Sea and Levant that have already reached a thermal steady state and thus are characterized by RT of -2 km to -3 km. In view of this typical path, the Afar Rift with its positive RT is exceptional indicating dynamic uplift. Another exception is the Ionian and Herodotus Basins (central Mediterranean), which are very deep relative to their crustal thickness with RT ranging from -3 km to -5 km. These forearc basins are clearly subduction related (SRFB, subduction-related forearc/foreland basins).

Stable Continents (SC) such as North Africa and Arabia with their “normal” 30- to 40-km-thick crust are with “normal” RT of -1.5 km to -2.5 km, as expected from a mature ML, not very different from old oceanic basins (OOB, Atlantic) and old rifted basins (ORB, Levant Basin and Black Sea). Anatolia and parts of the Ethiopian Plateau also have a normal crust (35–45 km thick), but their RT is higher (-1 km to zero). This can express a thermally eroded continent (TEC) with a thin ML, dynamic uplift, or a combination of the two. However, the positive RT in large parts of the Ethiopian plateau and SW Yemen (e.g., Sembroni et al., 2016) cannot be explained even with complete removal of the ML. These areas are thus named dynamically uplifted continents (DUC) similar to the nearby dynamically uplifted ocean (DUO, Gulf of Aden).

Continental regions with normal crustal thickness and RT lower than -2.5 km are the East European craton and the Mesopotamian basin (also part of the South Caspian Sea). Whereas old and cold continental cratons (CC) may be explained statically with exceptionally thick ML (e.g., Zoback and Mooney, 2003), the Mesopotamian Basin is clearly related to long-wavelength bending towards the Zagros (SRFB subduction-related forearc/foreland basins) as also indicated by the gradual tilting of the crystalline basement.

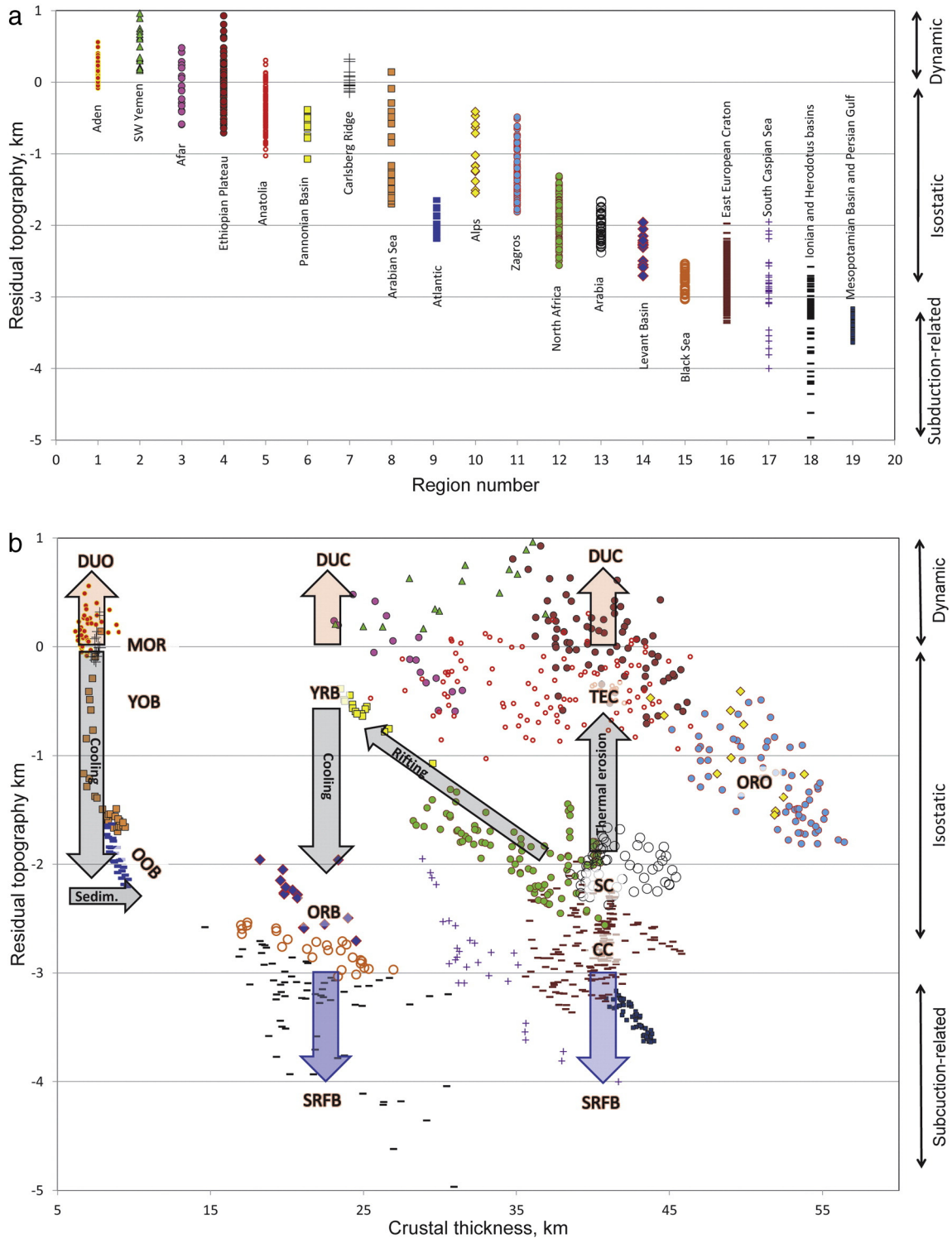


Fig. 8. Residual topography, tectonic environments, and processes controlling vertical motions. (a) Dependency relationships between residual topography and tectonic settings. (b) Residual topography of the same tectonic provinces as a function of crustal thickness. DUC—dynamically uplifted continent, DUO—dynamically uplifted ocean, MOR—mid-ocean ridge, YOB—young ocean basin, OOB—old ocean basin, YRB—young rifted basin, ORB—old rifted basin, SRFB—subduction-related foreland/forearc basin, TEC—thermally eroded continent, SC—stable continent, CC—cratonic continent, ORO, orogens.

The residual topography of orogens (ORO) with a thickened crust (e.g., Zagros and Alps) varies from -0.5 km to -2 km, which is a bit higher than old oceanic basins (OOB), old rifted basins (ORB), and stable continents (SC). The reason for that may be crustal thickening on account of the ML or root delamination (Houseman et al., 1981; Platt and England, 1994; Kay and Mahlburg Kay, 1993).

To summarize, (1) a mature ML generates a negative buoyancy producing RT of nearly -2 km as observed in old oceanic basins (OOB), old rifted basins (ORB), and stable continents (SC). (2) Positive RT in dynamically uplifted oceans (DUO, Aden) and dynamically uplifted continents (DUC, Ethiopian Plateau) clearly express dynamic upwelling (it is still not clear, however, if the ML at these regions is

completely absent). (3) High RT of -1 km to zero as observed in thermally eroded continents (TEC, Anatolia) probably indicates a thin ML, but dynamic uplift may also be involved. (4) Continental Cratons (CC) are associated with a thick ML and low RT of ~ -3 km. (5) Exceptionally low RT of less than -3 km is observed only in subduction-related basins within the forearc or foreland basins and even farther away (SRFB, Ionian, Herodotus, and Mesopotamia).

4. Discussion

4.1. Interpretation of residual topography

Topography is a first-order signal of Earth's dynamics; however, its interpretation is not straightforward as it results from the superposition of different signals. We often refer to isostatic and dynamic signals to

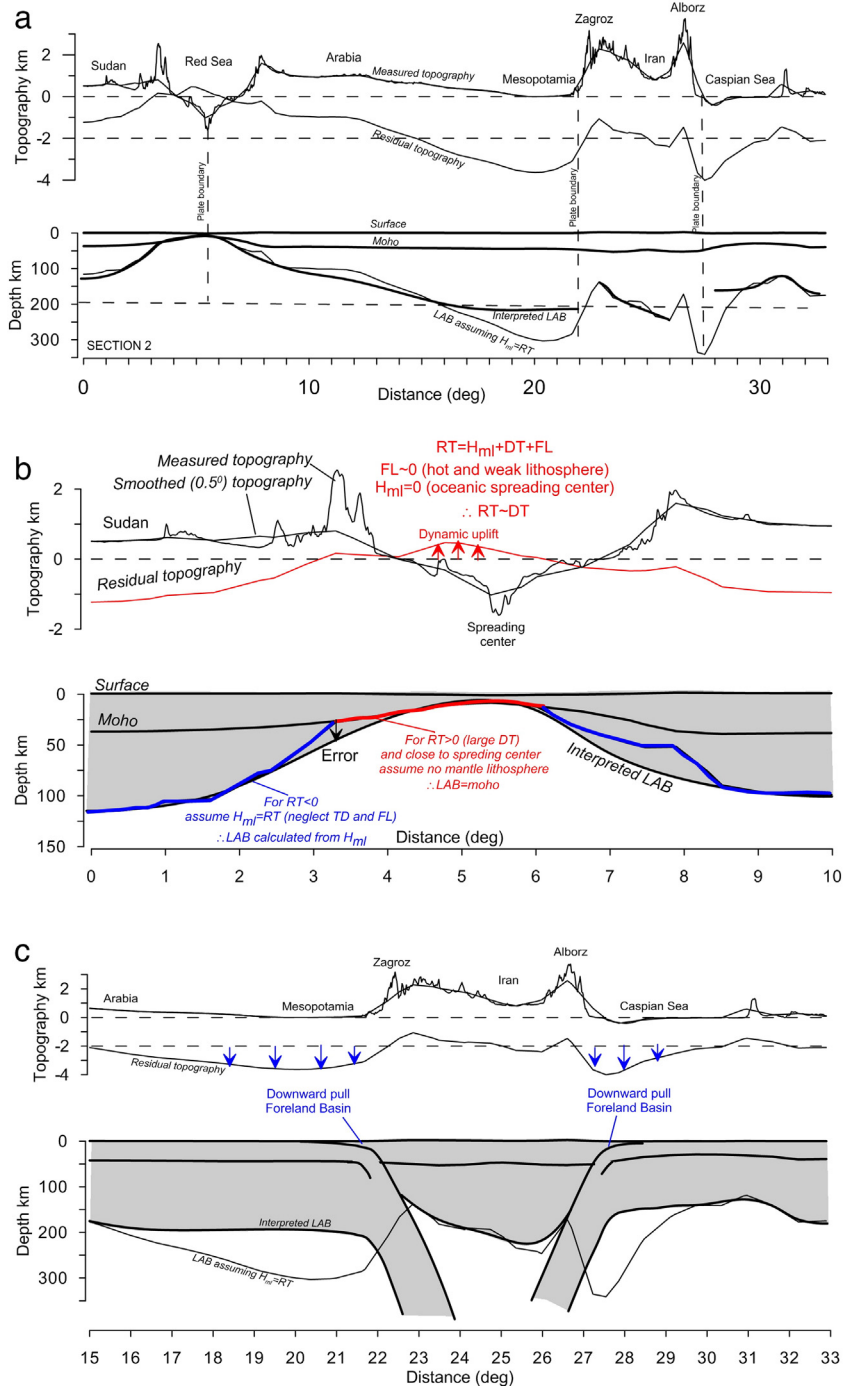


Fig. 9. Interpretation of residual topography illustrated on a cross-section from East Africa to the Caspian Sea (location on Figs. 1, 4). (a) Upper panel: measured, smoothed, and residual topography. Lower panel: crust and interpreted LAB. (b) Enlargement of the dynamically uplifted area, where the Afar mantle plume (max DT) coincides with the southern Red Sea spreading center ($H_{ml} = 0$). In this area, residual topography constrains the maximal dynamic uplift to ~ 1 km. For inferring the LAB, we practically assume $RT = DT$ where $RT > 0$ (LAB marked red) and $RT = H_{ml}$ for all the rest (blue). The error associated with such approximation is illustrated by a black arrow. (c) Enlargement of the Mesopotamian-Zagros and Caspian-Alborz foreland basins. Assuming that the mantle lithosphere does not thicken under foreland basins, the exceptionally low residual topography is interpreted as the downward-pulled subduction-related force exerted by far-off slab hanging below the orogen.

separate between the lithosphere's static contribution and the dynamic transient contribution related to mantle convection. Here, we investigate a region with different tectonic environments: mantle plume, convergent-collisional margin, subduction zone, spreading ridge, and stable cratonic areas. The goal is to provide a robust estimate of the isostatic and dynamic components. For simplicity, we first present an end member isostatic approach that interprets RT in terms of H_{ml} and L_{ml} limiting DT only to areas where isostasy alone cannot explain the observations (mantle plumes and subduction zones). Then, we discuss the error in L_{ml} associated with ignoring DT even when it is relatively small.

In reality, the lithosphere above upwelling plumes is hot, thin, and weak and the lithosphere above down-welling mantle flows is cold, strong, and with no indications for thinning. Accordingly, for regions with high residual topography, which are commonly associated with elevated heat flow and magmatism, we first assume that $DT > 0$ (mantle flow is upwards), $H_{ml} > -2$ km (ML is thinner than normal), and for topographic loads wider than ~ 100 km $FL \approx 0$ (lithosphere is weak). Second, we suggest to take advantage of the unique conjunction of a mantle plume and a mid-ocean ridge in the Gulf of Aden and the southern Red Sea (Fig. 6b). At this location, $H_{ml} = 0$, because the ML is absent along MOR, and DT is nearly maximal, because western Aden is located very close to the center of the plume (Fig. 9a,b). In other words, RT which is ~ 1 km in the southern Red Sea and western Aden, represents the regional maximal dynamic uplift ($RT = DT_{max} \sim 1$ km) consistent with dynamic topography prediction from present-day global mantle flow (Fig. 6e from Faccenna et al., 2014a) using the SAVANI S-wave model (Auer et al., 2014).

For foreland and forearc basins, we suggest that the exceptionally low residual topography does not indicate ML thickening because there is no reason to think that the (e.g., Arabian) ML thickens hundreds of kilometers before reaching the subduction plate boundary (e.g., Mesopotamia–Zagros line) (Fig. 9c). Hence, H_{ml} in Mesopotamia is similar to H_{ml} in Arabia (~ -2 km) and the lateral change from RT of ~ -2 km in Arabia to ~ -3.5 km in Mesopotamia is probably related to the subduction process as also indicated by the large negative free air anomaly (Fig. 2b). Similarly, in the Ionian and Herodotus basins, RT reaches -5 km and in the extreme case of the deep south Mariana trench (western Pacific), which is more than 5 km deeper than the adjacent abyssal plains, RT reaches a world maximum of ~ -7 km (Gvirtzman and Stern, 2004). These extremely low RT values definitely do not indicate thickening of the ML and, therefore, we suggest assuming that ML thickness at those areas is similar to ML thickness of the same plates farther back before reaching the area influenced by subduction.

Considering that in the vicinity of the Afar Plume, very close to Aden–Red Sea spreading centers, there is no ML; and considering that in foreland and forearc basins, the thickness of the ML is probably similar to its thickness in the unbent portion of the same plate, we focus the discussion on the ability to approximate ML thickness from RT on other regions (most of the study area). To begin this discussion, we now examine the consequences of neglecting DT and presuming isostasy. This actually means that in those areas, we assume $H_{ml} \approx RT$ and calculate the thickness of the ML using Eq. (8). Results of this first order approximation are shown in the lithospheric thickness map of Fig. 6d.

This exercise is further clarified by Fig. 7b, showing the relationships between ML thickness and ML contribution to topography for various ML densities and various tectonic environments. For instance, young oceanic basins fall on the 1000 °C Moho temperature and 3220 kg/m³ ML density; and old oceanic basins fall near the curve of 100 °C Moho temperature and 3270 kg/m³ ML density. Similarly, the Alps have a lighter ML than stable continents, because its Moho is deep and hot. Also, note that the East European craton is a cold region but its Moho temperature is not so cold because it is deep. On the contrary, the Ionian and Herodotus basins have a relatively dense ML because their Moho temperature is relatively shallow and cold. In general, Fig. 7b illustrates

that changes in ML density can affect the calculation of the ML thickness by ~ 50 km and thus cannot be neglected.

In the East European craton, the inferred thickness of the calculated ML is larger than 200 km and the entire lithospheric thickness reaches 250 km. This analysis assumes a pure thermal control on the ML for the sake of argument. However, the density of the ML may be significantly influenced by petrologic variations in continental lithosphere (e.g., Jordan, 1988; Forte and Perry, 2000; O'Reilly et al., 2001; Zoback and Mooney, 2003; Steinberger, 2016). Particularly highly fractionated mantle roots under cratons may be associated with a positive chemical buoyancy anomaly that offsets the negative thermal buoyancy (e.g., Jordan, 1988; Lee et al., 2005), implying that our calculation underestimates the thickness of the ML under cratons. Also, using a constant value for the density of the asthenosphere becomes problematic underneath thick continental lithosphere (e.g., Poudjom-Djomani et al., 2001).

The approach adopted here is to explore the possibility that most of the RT is due to intra-lithospheric buoyancy variations. A different perspective is demonstrated, for example, by Forte (2007), who calculate the expected topography variations resulting from lateral buoyancy differences in the upper 200 km of the mantle and, then, from buoyancy differences located below 200 km; in both cases, global-scale undulations of at least 1 km are obtained. In other words, modeling of mantle circulation shows that DT in regions far away from mantle plumes and forearc/foreland basins can be larger than ± 1 km. Examples for regions that do not coincide with simple, isolated mantle plumes or subduction zones and yet are strongly influenced by dynamic topography are Anatolia (Şengör et al., 2003; Boschi et al., 2010), South Africa (Lithgow-Bertelloni and Silver, 1998; Gurnis et al., 2000), Basin and Range (Hyndman and Currie, 2011; Lowry et al., 2000; Becker et al., 2014), and others.

These cases indicate that presuming isostasy even far away from mantle plumes and subduction zones is associated with an error and the question addressed now is how large this error is in the area studied here. For example, in the southern parts of Israel and Jordan, RT ranges between -0.6 and -0.7 km (Fig. 6b), whereas in the adjacent area of central Arabia, RT varies between a “normal” value of -2 km (this study) and a world average value of -1.7 km (Zoback and Mooney, 2003). The explanation for the 1.0 – 1.4 km anomaly in southern Israel and Jordan is most probably a combination of lithospheric thinning and dynamic support, yet what is the relative contribution of these two effects? Considering that the maximal value of DT just above the Afar Plume is only 1 km and that the Israel–Jordan area is located 2000 km away, the dynamic effect might decrease to a few hundred meters (100–300 m). Theoretically, the presence of an additional plume beneath Arabia (e.g., Daradich et al., 2003; Chang and Van der Lee, 2011) may increase the dynamic effect in Israel and Jordan. However, using $H_{ml} = RT$ and calculating ML thickness from Eq. (8), the total lithospheric thickness in the Jordan–Israel area is 70–80 km (Fig. 6d), quite similar to receiver function measurements indicating 60–80 km (Mohsen et al., 2006). Apparently, this supports the conclusion that DT in north Arabia is relatively small, because for such an area, 10–20 km in lithospheric thickness corresponds to 100–300 m in RT (Fig. 7b). Nonetheless, considering the widespread trace of volcanism (e.g., Coleman, 1993), dynamic contribution cannot be excluded even in north Arabia (Daradich et al., 2003; Becker and Faccenna, 2011; Faccenna et al., 2013).

4.2. Topography, lithospheric structure, mantle dynamics, and tectonic environments

We now return to the large scattering in the topography–crustal thickness diagram (Fig. 1) where the same crustal thickness is commonly accompanied by topographic variations of a few km. Our analysis shows that this scatter depends on the tectonic environment (Fig. 10a). Thus, considering this dependency together with available

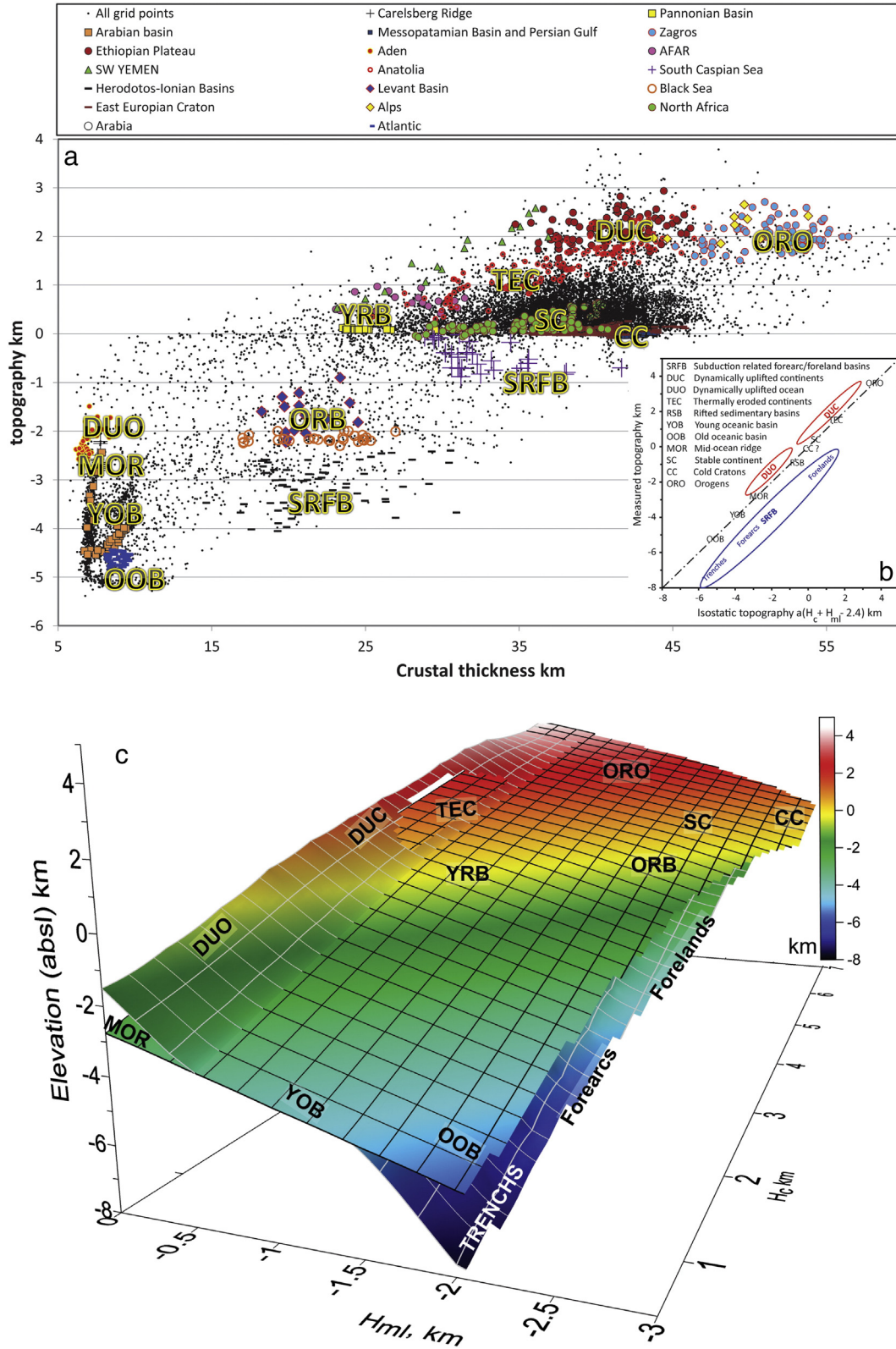


Fig. 10. (a) Elevation versus crustal thickness for all grid points in the study area (all black points) and particularly in the selected tectonic provinces (colored points; location in Fig. 2). Compared with the poor correlation between elevation and crustal thickness in Fig. 1, here we show that scattering is systematic and depends on the tectonic settings. (b) Expected correlation between observed and isostatically calculated topography for different tectonic environments. Whereas, for most environments (black), the expected error is in the order of a few hundred meters, in dynamically uplifted environments (red) and downward pulled subduction-related forearc and foreland basins (blue), deviation from isostasy may reach a few km. (c) 3D illustration of Earth's topography as a function of crustal and mantle lithosphere contributions to lithospheric buoyancy in isostatically balanced areas (less curved surface) and in dynamically affected zones (deflected surface). Subduction-related pull down-areas affect cold regions with thick lithosphere (right-hand side of the figure). Dynamically uplifted areas affect hot areas with a thin lithosphere (left-hand side). Note the difference between thermally eroded continents (TEC), where elevated topography results from lithospheric thinning and dynamically uplifted continents (DUC), where elevated topography is controlled by mantle upwelling. Abbreviations as in Fig. 8.

knowledge about crustal density and Moho temperature, we can identify regions where isostasy provides a fairly good approximation for the earth's topography and regions where isostasy does not work (Fig. 10b). We envisage that at those regions where isostasy works well; theoretically, topography can be predicted from lithospheric buoyancy given independent measurements of lithospheric thickness (e.g., receiver function measurements or surface waves LAB). Noteworthy, such measurements should be considered with caution because it is not always clear what is exactly measured (e.g., Fischer et al., 2010) and because the LAB is a gradual transition zone with several definitions (cf. Becker et al., 2014). Here, we compute the base of what we define as the *isostatic lithosphere*, which is similar to the buoyancy determined LAB (e.g., Gvirtzman and Nur, 1999, 2001; Zoback and Mooney, 2003). *Isostatic lithosphere* does not necessarily coincide with *mechanical lithosphere* (strong), *thermal lithosphere* (conductive), or *seismic lithosphere* (above the low velocity zone).

A useful way to generalize our results is to plot them along a schematic plate-tectonic section (Fig. 11d) including variety of tectonic environments and to accompany this section with profiles of all relevant parameters (crustal density, ML density, topography, H_c , and RT). This presentation illustrates several rules of thumb in a self-consistent manner. Crustal density varies by 300 kg/m^3 between 2650 kg/m^3 in sedimentary rich basins to 2950 kg/m^3 in oceanic basins (Fig. 11a). Disregarding possible compositional effects, changes in ML density are an order of magnitude lower, changing from 3220 kg/m^3 in hot Moho to 3270 kg/m^3 in cold Moho with low peaks (hot mantle) near oceanic

ridges, mantle plumes, and orogens (deep Moho) and high peaks in stretched continental basins and old oceans (shallow Moho) (Fig. 11b). Crustal contribution to topography (Fig. 11c, brown curve) is always higher than the actual topography (black). Residual topography is commonly around -2 km with low peaks in foreland basin and cratons and high peaks above upwelling plumes. Topographic highs are controlled by crustal thinning (extended basins), crustal thickening (orogen), thermal erosion (continental plateau), ML thickening (craton), flexure towards subduction zones (foreland basin), and dynamic support (continents and oceans).

Despite this analysis, interpretation of RT in many places remains ambiguous. For instance, in Anatolia and in Ethiopia, the distinction between ML thinning and dynamic topography (Fig. 8b) is not clear (Şengör et al., 2003; Boschi et al., 2010). These two signals of topography actually express the same phenomena of mantle upwelling that thermally thins the lithosphere and pushes it upwards (e.g., Becker and Faccenna, 2011; Faccenna et al., 2013, 2014a). The question discussed here is not the origin of these processes, but whether or not isostasy correctly accounts for thermal thinning of the lithosphere as it accounts for mechanical thinning of the lithosphere in extended sedimentary basins. Possible solution to this question may arise from quantitative examination of the history of vertical motions (paleotopography), but this is beyond the scope of this study.

Moving from uplifted continents to large oceanic basins, the uncertainty in DT may be reduced even far away from mantle plumes by comparing depth anomalies to age-dependent subsidence curves

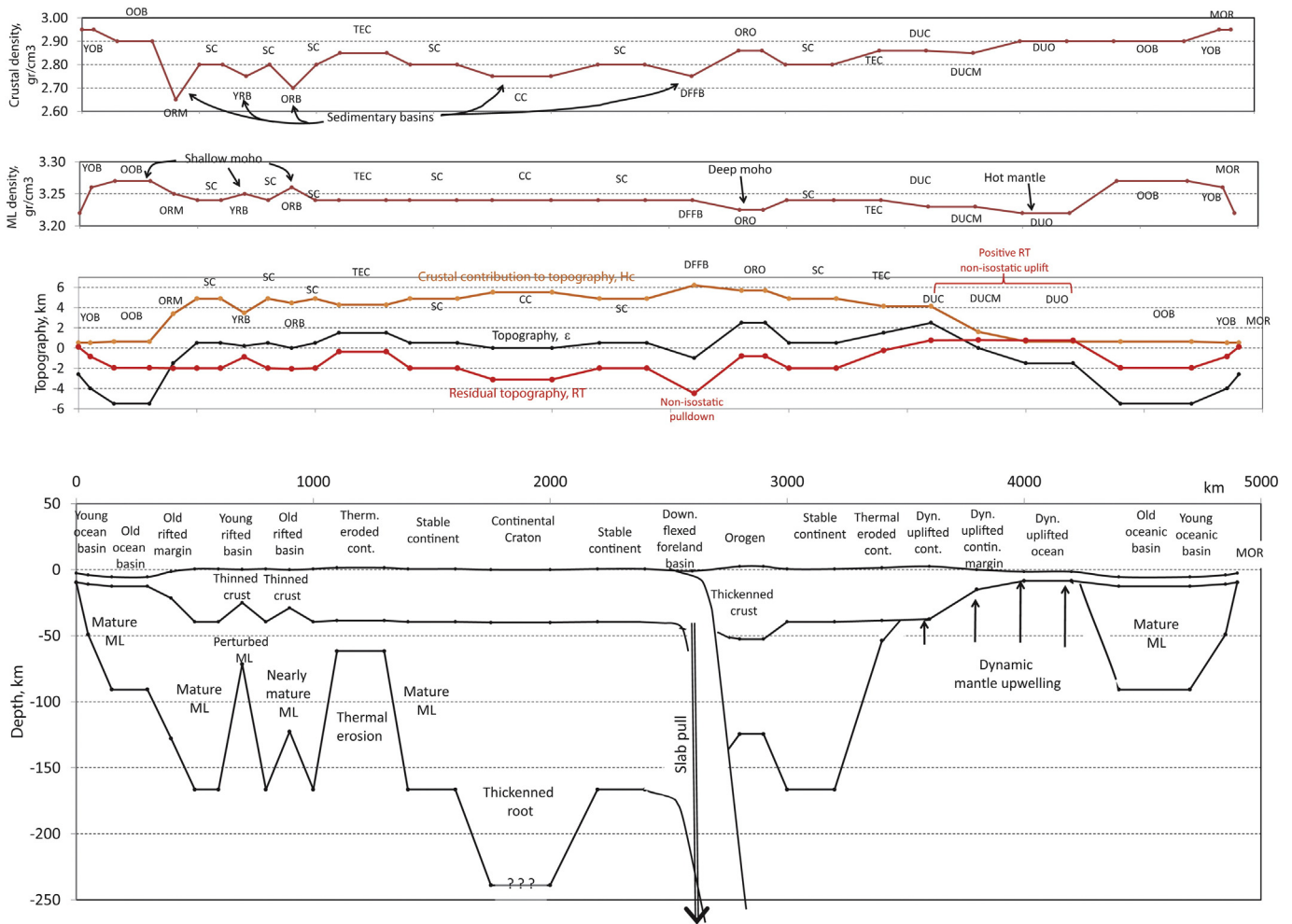


Fig. 11. A simplified plate-tectonic section including a variety of tectonic environments with typical profiles of crustal density, ML density, topography, crustal buoyancy, and residual topography, and areas of dynamic uplift and downward pull-down. This illustrates how isostasy works and where isostasy alone cannot explain the observations. Lithospheric thickness in cratons may be larger due to density variations related to petrological variations, which are not considered in this study

(Winterbourne et al., 2009; Crosby et al., 2006; Crosby and McKenzie, 2009). In addition, past fluctuations in DT may be reconstructed from stratigraphic evidence of major marine transgressions and regressions (e.g., Mitrovica et al., 1989; Gurnis, 1990a, 1990b; Gurnis, 1993; Bertelloni and Gurnis, 1997; Moucha et al., 2008; Müller et al., 2008; Sembroni et al., 2016), though here again, the distinction between lithospheric thinning and DT is not always clear.

5. Summary

The difficulty to predict topography from lithospheric structure or, alternatively, estimate lithospheric thickness from residual topography, results from two basic limitations. (1) Factors controlling lithospheric buoyancy in most parts of the world are uncertain, and (2) non-isostatic factors such as lithospheric bending and dynamic topography are hard to quantify. In this study, we suggest several steps to overcome these difficulties.

We examine systematic relationships between tectonic environments and factors controlling topography that support our understanding and encourage useful approximations. Considering that crustal thickness is a primary condition to our exercise, we re-examined all available data to compile a new Moho map for the area of the Red Sea–Middle East–Eastern Mediterranean. We suggest that crustal density can be approximated from its thickness (Moho maps are constantly improving), its origin (oceanic/continental), and its sedimentary cover (thickness and density data available from the oil industry). This approximation allows better calculation of the contribution of the crust to topography, and consequently, the residual topography.

We suggest that ML density can be approximated, to first order, from geothermal data and Moho depth. In isostatically supported regions, this approximation allows interpreting residual topography in terms of lithospheric thickness.

We constrain the amplitude of positive dynamic topography above the Afar plumes to be of ~1 km, representing a regional maximum in agreement with other studies (Sembroni et al., 2016). Within the study area, including northern Arabia, DT is relatively small and neglecting it is associated with an error of only 10–30 km in lithospheric thickness. This conclusion is supported by receiver function measurements of the LAB in southern Israel and Jordan.

We show that in foreland and forearc basins, where the lithosphere bends down, residual topography is extremely low (–2.5 km to –6 km). We argue that since down-going plates do not thicken before entering subduction, the extremely low residual topography in forearc/foreland basins express the slab pull-down force rather than lithospheric thickening. Taking lithospheric thickness under foreland/forearc basins from adjacent areas, the amplitude of two subduction-related effects (semi-static slab load and dynamic topography) is constrained. Distinction between these two effects is yet problematic.

Lastly, we present a simplified plate-tectonic section including a variety of tectonic environments with typical profiles of crustal density, ML density, topography, crustal buoyancy, and residual topography. This illustrates how isostasy works and where isostasy alone cannot explain the observations.

Supplementary data to this article can be found online at <http://dx.doi.org/10.1016/j.tecto.2016.05.041>.

Acknowledgements

This research was supported by a binational grant from the Ministry of Science & Technology (Israel) and the Ministry of Foreign Affairs (Italy). Claudio Faccenna was also supported by the ITN Topomod and PRIN projects. Thorsten W. Becker was partially supported by NSF EAR-1250214 and EAR-1338329. We are particularly grateful to Alessandro Forte and other two anonymous reviewers whose comments greatly improved our manuscript.

References

- Airy, G.B., 1855. On the computation of the effect of the attraction of mountain-masses, as disturbing the apparent astronomical latitude of stations in geodetic surveys. *Philos. Trans. R. Soc. Lond.* 101–104.
- Amante, C., Eakins, B.W., 2009. ETOPO1 1 Arc-Minute Global Relief Model: Procedures, Data Sources and Analysis NOAA Technical Memorandum NESDIS NGDC-24, p. 19.
- Artemieva, I.M., 2006. Global 1 × 1 thermal model TC1 for the continental lithosphere: implications for lithosphere secular evolution. *Tectonophysics* 416, 245–277.
- Auer, L., Boschi, L., Becker, T., Nissen-Meyer, T., Giardini, D., 2014. Savani: a variable resolution whole-mantle model of anisotropic shear velocity variations based on multiple data sets. *J. Geophys. Res. Solid Earth* 119, 3006–3034.
- Bar, O., Zilberman, E., Feinstein, S., Calvo, R., Gvirtzman, Z., 2016. The uplift history of the Arabian plateau as inferred from geomorphologic analysis of its northwestern edge. *Tectonophysics* 671, 9–23. <http://dx.doi.org/10.1016/j.tecto.2016.01.004>.
- Bassin, C., Laske, G., Masters, G., 2000. The current limits of resolution for surface wave tomography in North America. *EOS Trans AGU* F897.
- Becker, T.W., Faccenna, C., 2011. Mantle conveyor beneath the Tethyan collisional belt. *Earth Planet. Sci. Lett.* 310, 453–461.
- Becker, T.W., Faccenna, C., Humphreys, E.D., Lowry, A.R., Miller, M.S., 2014. Static and dynamic support of western United States topography. *Earth Planet. Sci. Lett.* 402, 234–246.
- Bertelloni, C.L., Gurnis, M., 1997. Cenozoic subsidence and uplift of continents from time-varying dynamic topography. *Geology* 25, 735–738.
- Boschi, L., Faccenna, C., Becker, T., 2010. Mantle structure and dynamic topography in the Mediterranean Basin. *Geophys. Res. Lett.* 37.
- Cazenave, A., Souriau, A., Dominh, K., 1989. Global coupling of Earth surface topography with hotspots, geoid and mantle heterogeneities. *Nature* 340, 54–57.
- Chang, S.-J., Van der Lee, S., 2011. Mantle plumes and associated flow beneath Arabia and East Africa. *Earth Planet. Sci. Lett.* 302, 448–454.
- Christensen, U.R., 1998. Dynamic phase boundary topography by latent heat effects. *Earth Planet. Sci. Lett.* 154, 295–306.
- Coleman, R., 1993. *Geologic Evolution of the Red Sea Oxford Monographs on Geology and Geophysics*. Oxford University Press, Oxford.
- Colin, P., Fleitout, L., 1990. Topography of the ocean floor: thermal evolution of the lithosphere and interaction of deep mantle heterogeneities with the lithosphere. *Geophys. Res. Lett.* 17, 1961–1964.
- Crosby, A., McKenzie, D., 2009. An analysis of young ocean depth, gravity and global residual topography. *Geophys. J. Int.* 178, 1198–1219.
- Crosby, A., McKenzie, D., Sclater, J., 2006. The relationship between depth, age and gravity in the oceans. *Geophys. J. Int.* 166, 553–573.
- Daradich, A., Mitrovica, J.X., Pysklywec, R.N., Willett, S.D., Forte, A.M., 2003. Mantle flow, dynamic topography, and rift-flank uplift of Arabia. *Geology* 31, 901–904.
- Davies, G.F., 1979. Thickness and thermal history of continental crust and root zones. *Earth Planet. Sci. Lett.* 44, 231–238.
- Djomani, Y.H.P., O'Reilly, S.Y., Griffin, W.L., Morgan, P., 2001. The density structure of sub-continental lithosphere through time. *Earth Planet. Sci. Lett.* 184 (3), 605–621.
- Dutton, C., 1882. *Physics of the Earth's crust; by the Rev. Osmond Fisher*. *Amer. J. Science* 23, 283–290.
- Faccenna, C., Becker, T.W., 2010. Shaping mobile belt from small scale convection. *Nature* 465. <http://dx.doi.org/10.1038/nature09064>.
- Faccenna, C., Becker, T.W., Jolivet, L., Keskin, M., 2013. Mantle convection in the Middle East: reconciling Afar upwelling, Arabia indentation and Aegean trench rollback. *Earth Planet. Sci. Lett.* 375, 254–269.
- Faccenna, C., Becker, T.W., Auer, L., Billi, A., Boschi, L., Brun, J.P., Capitanio, F.A., Funicello, F., Horváth, F., Jolivet, L., 2014a. Mantle dynamics in the Mediterranean. *Rev. Geophys.* <http://dx.doi.org/10.1002/2013RG000444>.
- Faccenna, C., Becker, T.W., Miller, M.S., Serpelloni, E., Willett, S.D., 2014b. Isostasy, dynamic topography, and the elevation of the Apennines of Italy. *Earth Planet. Sci. Lett.* 407, 163–174.
- Fischer, K.M., Ford, H.A., Abt, D.L., Rychert, C.A., 2010. The lithosphere–asthenosphere boundary. *Annu. Rev. Earth Planet. Sci.* 38, 551–575.
- Flament, N., Gurnis, M., Müller, R.D., 2013. A review of observations and models of dynamic topography. *Lithosphere* 5, 189–210.
- Forte, A.M., 2007. 1.23—Constraints on Seismic Models from Other Disciplines—Implications for Mantle Dynamics and Composition. In: Schubert, G. (Ed.), *Treatise on Geophysics*. Elsevier, Amsterdam, pp. 805–858.
- Forte, A.M., Perry, H.C., 2000. Geodynamic evidence for a chemically depleted continental tectosphere. *Science* 290, 1940–1944.
- Forte, A., Peltier, W., Dziewonski, A., Woodward, R., 1993. Dynamic surface topography: a new interpretation based upon mantle flow models derived from seismic tomography. *Geophys. Res. Lett.* 20, 225–228.
- Forte, A.M., Quéré, S., Moucha, R., Simmons, N.A., Grand, S.P., Mitrovica, J.X., Rowley, D.B., 2010. Joint seismic–geodynamic–mineral physical modelling of African geodynamics: a reconciliation of deep-mantle convection with surface geophysical constraints. *Earth Planet. Sci. Lett.* 295, 329–341.
- Grad, M., Tiira, T., 2009. The Moho depth map of the European Plate. *Geophys. J. Int.* 176, 279–292.
- Gurnis, M., 1990a. Bounds on global dynamic topography from Phanerozoic flooding of continental platforms. *Nature* 344, 754–756.
- Gurnis, M., 1990b. Ridge spreading, subduction, and sea level fluctuations. *Science* 250, 970–972.
- Gurnis, M., 1993. Comment on “Dynamic surface topography: a new interpretation based upon mantle flow models derived from seismic tomography” by AM Forte, WR Peltier, AM Dziewonski and RL Woodward. *Geophys. Res. Lett.* 20, 1663–1664.
- Gurnis, M., Müller, R.D., Moresi, L., 1998. Cretaceous vertical motion of Australia and the Australian–Antarctic discordance. *Science* 279, 1499–1504.

- Gurnis, M., Mitrovica, J.X., Ritsema, J., van Heijst, H.J., 2000. Constraining mantle density structure using geological evidence of surface uplift rates: the case of the African superplume. *Geochem. Geophys. Geosyst.* 1.
- Gvirtzman, Z., Nur, A., 1999. Plate detachment, asthenosphere upwelling, and topography across subduction zones. *Geology* 27, 563–566.
- Gvirtzman, Z., Nur, A., 2001. Residual topography, lithospheric structure and sunken slabs in the central Mediterranean. *Earth Planet. Sci. Lett.* 187, 117–130.
- Gvirtzman, Z., Stern, R.J., 2004. Bathymetry of Mariana trench-arc system and formation of the Challenger Deep as a consequence of weak plate coupling. *Tectonics* 23.
- Hager, B.H., Clayton, R.W., Richards, M.A., Comer, R.P., Dziewonski, A.M., 1985. Lower mantle heterogeneity, dynamic topography and the geoid. *Nature* 313, 541–545.
- Haxby, W.F., Turcotte, D.L., 1978. On isostatic geoid anomalies. *J. Geophys. Res. Solid Earth* 83, 5473–5478.
- Heiskanen, W., Vening Meinesz, F.A., 1958. *The Earth and Its Gravity Field*. McGraw, NY.
- Houseman, G.A., McKenzie, D.P., Molnar, P., 1981. Convective instability of a thickened boundary layer and its relevance for the thermal evolution of continental convergent belts. *J. Geophys. Res.* 86, 6115–6132.
- Hyndman, R., Currie, C., 2011. Why is the North America Cordillera high? Hot backarcs, thermal isostasy, and mountain belts. *Geology* 39, 783–786.
- Jordan, T.H., 1988. Structure and formation of the continental tectosphere. *J. Petrol.* (1), 11–37.
- Kay, R.W., Mahlburg Kay, S., 1993. Delamination and delamination magmatism. *Tectonophysics* 219, 177–189.
- Lachenbruch, A.H., Morgan, P., 1990. Continental extension, magmatism and elevation; formal relations and rules of thumb. *Tectonophysics* 174, 39–62.
- Laske, G., Masters, G., Ma, Z., Pasyanos, M., 2013. Update on CRUST1.0-A 1-degree Global Model of Earth's Crust. EGU General Assembly Conference Abstracts, p. 2658.
- Le Stunff, Y., Ricard, Y., 1995. Topography and geoid due to lithospheric mass anomalies. *Geophys. J. Int.* 122, 982–990.
- Lee, C.-T.A., Lenardic, A., Cooper, C.M., Niu, F., Levander, A., 2005. The role of chemical boundary layers in regulating the thickness of continental and oceanic thermal boundary layers. *Earth Planet. Sci. Lett.* 230, 379–395.
- Lithgow-Bertelloni, C., Silver, P.G., 1998. Dynamic topography, plate driving forces and the African superswell. *Nature* 395, 269–272.
- Lowry, A.R., Ribe, N.M., Smith, R.B., 2000. Dynamic elevation of the Cordillera, western United States. *J. Geophys. Res. Solid Earth* 1978–2012 (105), 23371–23390.
- Milner, K., Becker, T.W., Boschi, L., Sain, J., Schorlemmer, D., Waterhouse, H., 2009. The Solid Earth Research and Teaching Environment: a new software framework to share research tools in the classroom and across disciplines. *Eos Trans. AGU* 90, 12. <http://dx.doi.org/10.1029/2009EO120005>.
- Mitrovica, J., Beaumont, C., Jarvis, G., 1989. Tilting of continental interiors by the dynamical effects of subduction. *Tectonics* 8, 1079–1094.
- Mohsen, A., Kind, R., Sobolev, S.V., Weber, M., 2006. Thickness of the lithosphere east of the Dead Sea Transform. *Geophys. J. Int.* 167, 845–852.
- Mooney, W.D., Laske, G., Masters, T.G., 1998. CRUST 5.1: a global crustal model at 5×5 . *J. Geophys. Res. Solid Earth* 1978–2012 (103), 727–747.
- Mooney, W.D., Prodehl, C., Pavlenkova, N., 2002. Seismic velocity structure of the continental lithosphere from controlled source data. *Int. Geophys. Ser.* 81, 887–910.
- Moucha, R., Forte, A.M., 2011. Changes in African topography driven by mantle convection. *Nat. Geosci.* 4, 707–712.
- Moucha, R., Forte, A.M., Mitrovica, J.X., Rowley, D.B., Quere, S., Simmons, N.A., Grand, S.P., 2008. Dynamic topography and long-term sea-level variations: there is no such thing as a stable continental platform. *Earth Planet. Sci. Lett.* 271, 101–108.
- Müller, R.D., Sdrolias, M., Gaina, C., Steinberger, B., Heine, C., 2008. Long-term sea-level fluctuations driven by ocean basin dynamics. *Science* 319, 1357–1362.
- O'Reilly, S., Griffin, W., Poudjom Djomani, Y., Morgan, P., 2001. Are lithospheres forever. Tracking changes in subcontinental lithospheric mantle through time. *GSA Today* 11, pp. 4–10.
- Panasyuk, S.V., Hager, B.H., 2000. Inversion for mantle viscosity profiles constrained by dynamic topography and the geoid, and their estimated errors. *Geophys. J. Int.* 143, 821–836.
- Parsons, B., Sclater, J.G., 1977. An analysis of the variation of ocean floor bathymetry and heat flow with age. *J. Geophys. Res.* 82, 803–827.
- Platt, J., England, P., 1994. Convective removal of lithosphere beneath mountain belts; thermal and mechanical consequences. *Am. J. Sci.* 294, 307–336.
- Royden, L.H., 1993. The tectonic expression slab pull at continental convergent boundaries. *Tectonics* 12, 303–325.
- Sandwell, D.T., Smith, W.H., 2009. Global marine gravity from retracked Geosat and ERS-1 altimetry: Ridge segmentation versus spreading rate. *J. Geophys. Res. Solid Earth* 1978–2012, 114.
- Sembroni, A., Faccenna, C., Becker, T.W., Molin, P., Abebe, B., 2016. Longterm, deep-mantle support of the Ethiopia–Yemen Plateau. *Tectonics* 35, 469–488. <http://dx.doi.org/10.1002/2015TC004000>.
- Şengör, A., Özeren, S., Genç, T., Zor, E., 2003. East Anatolian high plateau as a mantle-supported, north-south shortened domal structure. *Geophys. Res. Lett.* 30.
- Speranza, F., Minelli, L., Pignatelli, A., Chiappini, M., 2012. The Ionian Sea: the oldest in situ ocean fragment of the world? *J. Geophys. Res. Solid Earth* 1978–2012, 117.
- Steinberger, B., 2016. Topography Caused by Mantle Density Variations: Observation-Based Estimates and Models Derived from Tomography and Lithosphere Thickness.
- Thompson, G.A., Talwani, M., 1964. Geology of the crust and mantle, Western United States. *Science* 146, 1539–1549.
- Thoraval, C., Machetel, P., Cazenave, A., 1995. Locally Layered Convection Inferred from Dynamic Models of the Earth's Mantle.
- Watts, A.B., 2001. *Isostasy and Flexure of the Lithosphere*. Cambridge University Press.
- Winterbourne, J., Crosby, A., White, N., 2009. Depth, age and dynamic topography of oceanic lithosphere beneath heavily sedimented Atlantic margins. *Earth Planet. Sci. Lett.* 287, 137–151.
- Zoback, M.L., Mooney, W.D., 2003. Lithospheric buoyancy and continental intraplate stresses. *Int. Geol. Rev.* 45, 95–118.